



Investigation on circumferential characteristics distribution in wavy-annular flow transition based on PLIF

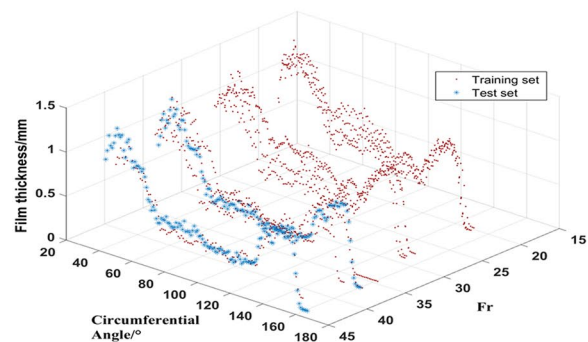
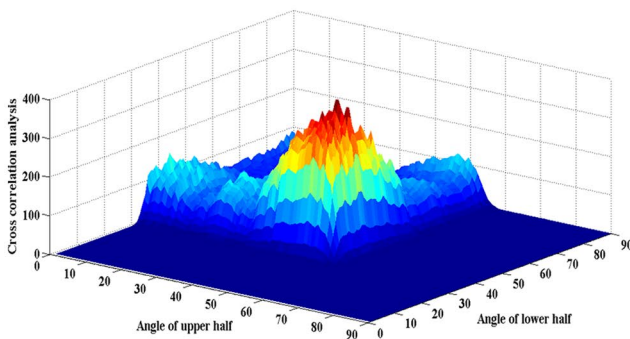
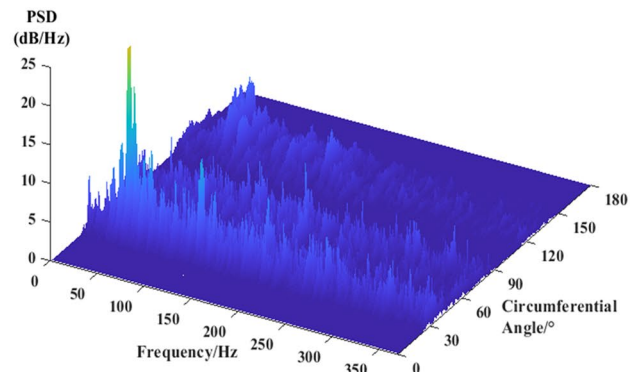
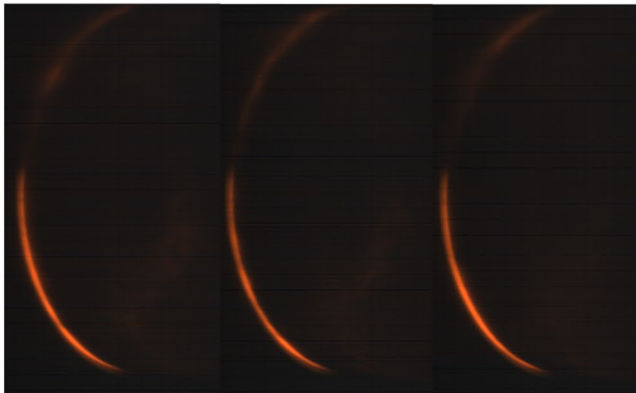
Ting Xue¹ · Tao Zhang¹ · Chenyang Li¹ · Zhuping Li¹

Received: 27 July 2021 / Revised: 19 January 2022 / Accepted: 19 January 2022 / Published online: 22 February 2022
© The Author(s), under exclusive licence to Springer-Verlag GmbH Germany, part of Springer Nature 2022

Abstract

With the excellent heat and mass transfer performance, the annular flow has been widely employed in industries. The study on the flow characteristics distribution of annular flow is the basis for revealing the flow mechanism and improving the performance. In this paper, based on the non-invasive planar laser-induced fluorescence technology, the circumferential characteristics of liquid film in horizontal annular flow and wavy flow are investigated. The circumferential film thickness and entrainment concentration are measured by the image processing. The spatial-temporal flow structure is reconstructed, and the cross-correlation analysis is conducted. The results show that the liquid entrainment and deposition phenomena contribute to the liquid film formation near the top of the pipe. In addition, a model which predicts the circumferential film thickness according to Froude number and circumferential angle is established.

Graphical abstract



✉ Ting Xue
xueting@tju.edu.cn

Extended author information available on the last page of the article

1 Introduction

In gas–liquid annular flow, the liquid flows along the pipe wall while the gas flows in the center of the pipe where droplets are entrained. Owing to the excellent heat and mass transfer properties, the annular flow is widely employed in chemical industry, petroleum industry, metallurgy, aerospace, and nuclear industry. Because of the gravity, the horizontal annular flow is characterized by a thin liquid film on the top of the pipe and a thicker liquid film on the bottom of the pipe, which affects the heat and mass transfer performance deeply. For example, the top of the pipe may not be wet in some conditions, which leads to dangers of burning in the cooling process. To avoid the risks and better utilize the performance of heat and mass transfer, it is necessary to measure the circumferential characteristics and analyze the mechanism of forming a steady liquid film in horizontal pipes, especially at the top of the pipe.

On account of the important industrial applications, the model of circumferential liquid film thickness asymmetry has been studied by Schubring et al. (2009), Cioncolini et al. (2013), Setyawan et al. (2017), and Layssac et al. (2017), which can be utilized to reduce asymmetry or prevent liquid film from becoming asymmetric in industrial design. In addition, the inclination effects on circumferential film distribution in annular gas–liquid flows have been investigated by Geraci et al. (2007) and Al-Sarkhi et al. (2012). The entrained droplets in the horizontal annular flow are more complicated than that of the vertical pipe. The droplet deposition rate has the same asymmetric distribution as the liquid film thickness, and the influence of gravity on the asymmetric distribution of droplets increases with increasing pipe inclination from vertical to horizontal. The heat and mass transfer performance is affected by the asymmetry distribution of liquid film thickness and droplet. Kattan et al. (1998) found that the dry prediction model was a function of the heat flux and flow parameters, which was depended on the film thickness distribution in horizontal pipe. Mauro et al. (2014) simulated the circumferential distribution of the liquid film and the heat transfer process of the annular flow during boiling process and found that the heat transfer efficiency from the top liquid film to the bottom liquid film differed by 25–30%.

Attempts have also been made to interpret the formation of the top liquid film in horizontal pipes. Anderson et al. (1970) found that the liquid film in annular two-phase flow was maintained by droplet movement to and from the gas core and by wave action. Laurinat et al. (1985) considered that the secondary flow was the cause of the top liquid film, and the measurement results obtained by Lin et al.

(1985) were highly consistent with the Laurinat model. However, Fukano et al. (1989) measured the horizontal annular flow and concluded that the effects of secondary flow were overestimated in the Laurinat model. They proposed a liquid film formation model which did not take the influence of secondary flow into consideration. It was regarded that the deposition of droplets and the pumping action of waves were the main causes of the formation for the liquid film on top of the pipe, and the measurement results were more consistent with the new model. Nevertheless, Westende et al. (2007) studied the effects of secondary flow in annular flow based on the numerical simulation. The results showed that the secondary flow was opposite to the direction of gravity, which represented that the secondary flow was a main cause of the formation of the top liquid film. The Fourier analysis of the film thickness at different circumferential locations was applied to obtain the disturbance wave characteristics by Setyawan et al. (2017), which supports that the liquid film in the upper part of the pipe is formed by the wave spreading. At present, the formation mechanism of the liquid film near the top of pipe is still not clear. The circumferential characteristics measurement is the key to comprehend and interpret the mechanism.

The liquid film thickness in annular flow is typically measured by the conductivity probes. Due to the advantages of non-invasive and high temporal-spatial resolution, laser-induced fluorescence (LIF) is more and more developed to the liquid film measurement, which includes planar laser-induced fluorescence (PLIF) and brightness-based laser-induced fluorescence (BBLIF). The evolution of ripples and disturbance waves has been investigated based on BBLIF by Alekseenko et al. (2008), Alekseenko et al. (2012, 2014), and An et al. (2020). A longer region of interrogation has been obtained along the test section. The wavy structure of liquid film in the annular flow based on PLIF has been investigated by Schubring et al. (2010a), Schubring et al. (2010b), and Zadrazil et al. (2014a). Xue et al. (2018) measured and analyzed the temperature field distribution of vertical falling film based on PLIF. Morgan et al. (2013) and Zadrazil et al. (2014b) considered the velocity field in waves with a combination of PLIF and particle image velocimetry (PIV), providing unique insight into annular flow. The distortion caused by refractive index mismatch and total reflection in PLIF images has been analyzed and corrected by Morgan et al. (2012), Haber et al. (2015), Eckeveld et al. (2018), Cherdantsev et al. (2019), and Charogiannis et al. (2019). PLIF has also been employed to provide the cross-sectional images of the liquid film. Farias et al. (2012) and Xue et al. (2017) measured the circumferential liquid film using two cameras and the virtual binocular view sensor, respectively. In addition, the studies of the distortion of circumferential liquid film

in annular flow have been carried out by Xue et al. (2019a) and Xue et al. (2019b).

In this paper, the circumferential characteristics distribution of horizontal annular flow is measured based on PLIF. According to image processing, the circumferential characteristics are extracted accurately. The time–frequency domain analysis is carried out, and the formation mechanism of the liquid film near the top of the horizontal pipe is investigated. It is found that entrainment droplets contribute to maintaining the liquid film near the top of the pipe, and a distribution model of the circumferential film thickness is established.

2 Circumferential liquid film measurement facilities setup

The gas–liquid annular flow measurement platform is shown in Fig. 1. The experiments are conducted in a flow loop, and the test section is constructed by the transparent acrylic pipe of 25 mm inner diameter. Air enters pipe at one end from the gasholder and then mixes with the liquid in gas–liquid mixer. After passing through the pipe and the test section, the air and water mixture is separated in a water tank. Water is pumped back to the pipe by a recirculating pump, and air is released to the atmosphere. The water flow rate is measured by a magnetic flowmeter with an accuracy of $\pm 0.5\%$, and the air flow rate is measured by a turbine flowmeter with an accuracy of $\pm 1.5\%$. Rhodamine B is added into the liquid phase, and the concentration is approximately 10 mg/L. With the laser sheet, the liquid film is excited to emit orange-red fluorescence on the circumferential section of the horizontal pipe. The liquid film is recorded by a high-speed camera equipped with filter; therefore, the fluorescence is retained. The length from the test section inlet to the measuring

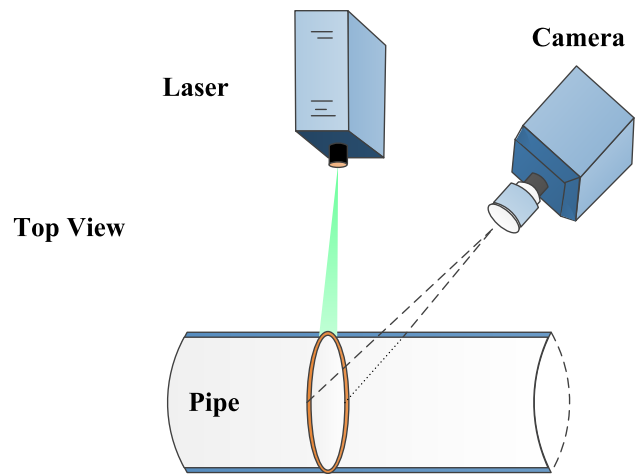
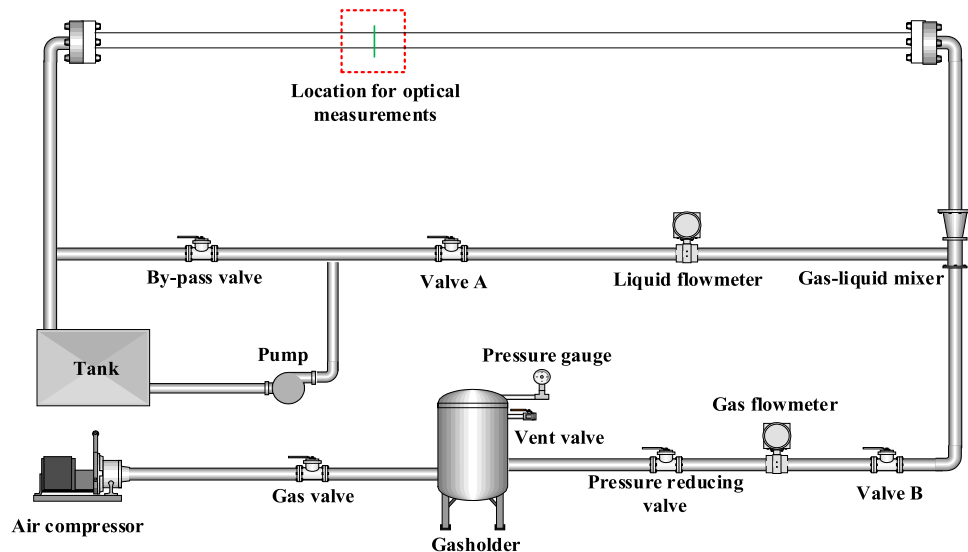


Fig. 2 Circumferential film imaging based on PLIF

location is about 3.6 m, so the dimensionless distance of liquid film thickness measuring location is 144, and the similar dimensionless distance has been applied by Fukano et al. (1989), Jayanti et al. (1990), and Li et al. (1999). As shown in Fig. 2, the laser and the camera are located in the same horizontal plane as the pipe, and the camera is set inclined to the pipe. The spatial resolution of the camera is $41 \mu\text{m}/\text{pixel}$ in both the axial and the radial directions, and the frame rate is set to 400 Hz. Due to the limitation of the field of view and the position of the camera, the measurable circumferential range is about $20\text{--}160^\circ$.

According to the flow pattern map (Mandhane et al. 1974), the gas–liquid flow rate is adjusted to make sure the flow pattern is about the annular flow, as shown in Fig. 3. The U_{sg} and U_{sl} are the superficial velocities of gas and liquid, respectively. To analyze the formation of the liquid film

Fig. 1 Experiment setup



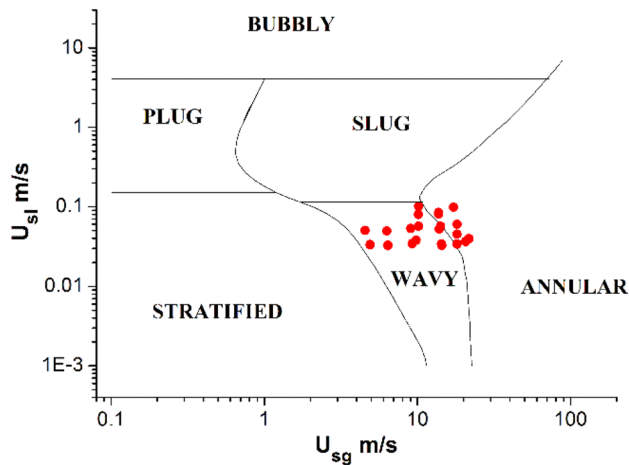


Fig. 3 The investigated flow conditions

Table 1 The gas and liquid superficial velocities

Run	U_{sg} (m/s)	U_{sl} (m/s)	Run	U_{sg} (m/s)	U_{sl} (m/s)
1	4.9	0.033	12	10.2	0.101
2	6.4	0.033	13	14.3	0.034
3	9.3	0.035	14	14.2	0.057
4	14.4	0.033	15	13.7	0.081
5	4.6	0.050	16	13.7	0.085
6	6.3	0.049	17	17.2	0.098
7	9.0	0.053	18	18.2	0.034
8	13.9	0.052	19	18.2	0.060
9	9.8	0.038	20	18.2	0.045
10	10.2	0.057	21	20.7	0.037
11	10.1	0.080	22	21.7	0.040

near the top of the pipe, both the wavy flow and the annular flow are measured in this paper (Table 1).

3 Circumferential film image processing

The image processing is shown in Fig. 4. As the gas superficial velocity increases, the flow pattern transits from the wavy flow to the annular flow. In Fig. 4a, the image above is the original image of the wavy flow, and the image below is the original image of the annular flow. The light from the liquid film on the other side of the pipe may be received after passing through the gas–liquid interface. Due to the fluctuation randomness of the gas–liquid interface, the distorted light path by the gas–liquid interface cannot be corrected. The image near the center of the pipe in the wavy flow is actually the image of glowing liquid film on the other side of the pipe, which is captured through the liquid film and extremely distorted. Therefore, the image near the center of

the pipe in the wavy flow is excluded when circumferential features are extracted. Due to the high gas superficial velocity, the liquid film in the annular flow is thinner than that in the wavy flow, which leads to a dim film image for the annular flow. It can be observed that the liquid film does not totally appear all along the pipe wall in the wavy flow, where the film adhered on the top of the pipe is much thinner than that on the bottom, and part of the pipe wall is not wet. However, in annular flow, the liquid film distribution is more symmetrical, and the entrainment is difficult to be observed. The following steps are employed to make sure the film thickness can be extracted accurately from the images.

3.1 Image processing and segmentation

As shown in Fig. 4b, the RGB color space is converted to the HSI color space, and the images are filtered. The fluorescence emitted by the liquid film is intensive in the frequency domain. The wave length of the fluorescence is about 570 nm. In HSI color space, only the colors whose wave length is close to the fluorescence are reserved, and the saturation of these colors is limited. The threshold values used in the color conversion are robust to the different liquid film images. After the color conversion, the time–frequency filtering is conducted to the converted images. A 3×3 Gaussian filter and a low pass filter are adopted to restrain the noise.

To obtain the film thickness, the image segmentation needs to be carried out to mark different flow structure. In Fig. 4c, the filtered images are judged before image segmentation, which are classified according to the flow patterns. The filtered annular flow images are segmented by the Otsu algorithm, which is shown below in Fig. 4c. The wavy flow images are segmented by the fuzzy C-means clustering algorithm, as shown above in Fig. 4c.

For horizontal pipes, a series of waves appear on the gas–liquid interface because the velocity difference between the gas and liquid phases increases during the transition from wavy flow to annular flow. As described by Berna et al. (2014), when the difference is high enough, the water droplets are extracted from the crest of these waves and then transported into the gas core by the gas stream with high velocity. Therefore, the waves covering the gas–liquid interface are considered to be related to the entrainment and deposition. In addition, Anderson et al. (1970), Laurinat et al. (1985), Fukano et al. (1989), Westende et al. (2007) and Setyawan et al. (2017) have attempted to interpret the formation of the top liquid film in the horizontal pipes. The possible causes of the formation of the top liquid film mainly include the entrainment and deposition phenomena, the pumping action of the waves, the secondary flow, and the wave spreading. However, the liquid film does not totally appear all along the pipe wall in the wavy flow, and the

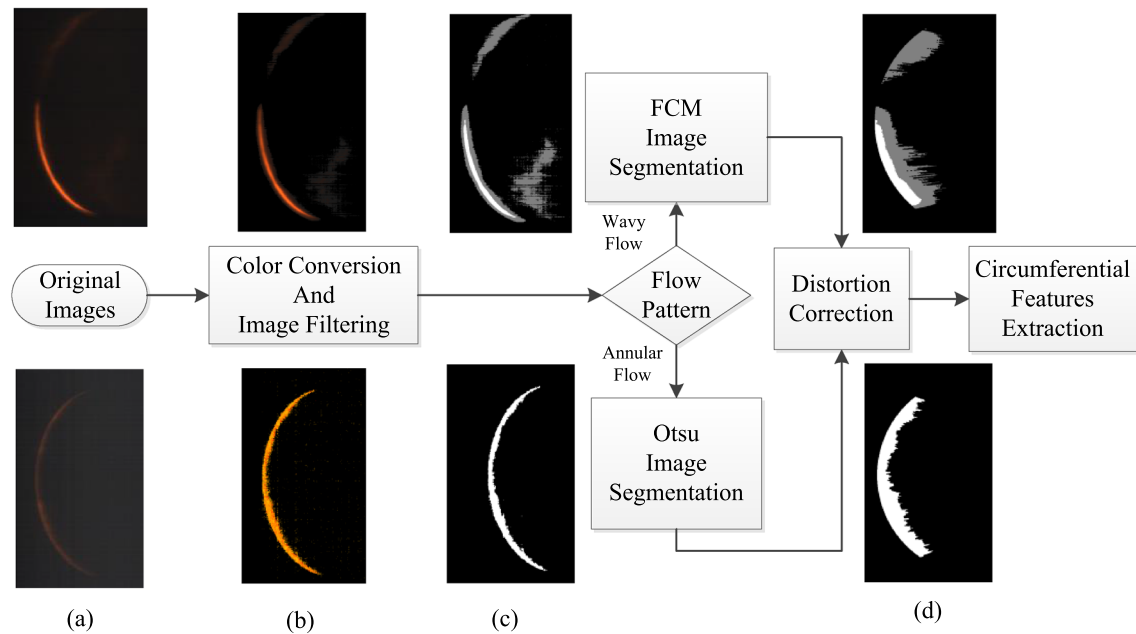


Fig. 4 Circumferential film image processing

fluorescence brightness near the top of the pipe is different from that at the bottom of the pipe, which means that the liquid film is not transported to the top of the pipe by the disturbance wave in transition flow pattern. Therefore, the waves at the top of the pipe are also considered to be related to the entrainment and deposition. The thickness of these areas is considered to be related to entrainment and deposition, which is defined as the entrainment concentration. The number of the clustering centers is set to be 3, which represents the background (grayscale: 0), the entrainment (grayscale: 128) and the liquid film (grayscale: 255), respectively.

3.2 Distortion correction

Due to the circular shape of the apparent pipe and the differences in refractive index, the light is deflected when it goes through the pipe wall, which leads to the distortion in film images. Aiming at the distortion in circumferential film measurement based on PLIF, Xue et al. (2019b) proposed an optical path analysis method, which corrects the distortion without any additional devices. In this paper, the correction method is employed, and the segmented images are corrected as shown in Fig. 4d. To verify the correction method, a static experiment is carried out. A frustum is placed into the transparent acrylic pipe with an inner and outer diameter of 25 mm and 35 mm. Its diameters of the upper and lower surfaces are 10 mm and 30 mm, respectively, and the height is 10 mm. The gap between the pipe and the frustum is filled with liquid phase to form liquid film. With the laser sheet,

the circumferential liquid film is excited to emit orange-red fluorescence. The distorted circumferential liquid film image is recorded by a camera at 45° to the pipe, and the distorted image is shown in Fig. 5a. According to the geometric relationship between the frustum and the pipe, the thickness of the circumferential liquid film can be calculated as a reference thickness. The circumferential liquid film is corrected, and the thickness of the liquid film is extracted. Figure 5b shows that most of the errors are within 5% and the average error is within 10% in the measurement range.

To analyze the effect of total internal reflection, a waveless annular film with uniform thickness was considered first, as shown in Fig. 6a. When the angle between the camera and the pipe is 45° , the reflection angle of light at the gas–liquid interface is 32° , which is less than the critical total reflection angle of 48.7° . In addition to this analysis, parameters such as the film thickness, wave curvature and height were considered in simplified 2-D simulations in an effort to understand the influence of total reflection, as shown in Fig. 6b. The results show that total reflection may occur in some cases when the gas–liquid interface fluctuates but not in others; therefore, it is assumed in this work that the effect is small.

3.3 Circumferential features extraction

The film thickness is extracted along the different circumferential directions as shown in Fig. 7. The axis center is set to be the origin of the coordinate, and γ is the circumferential

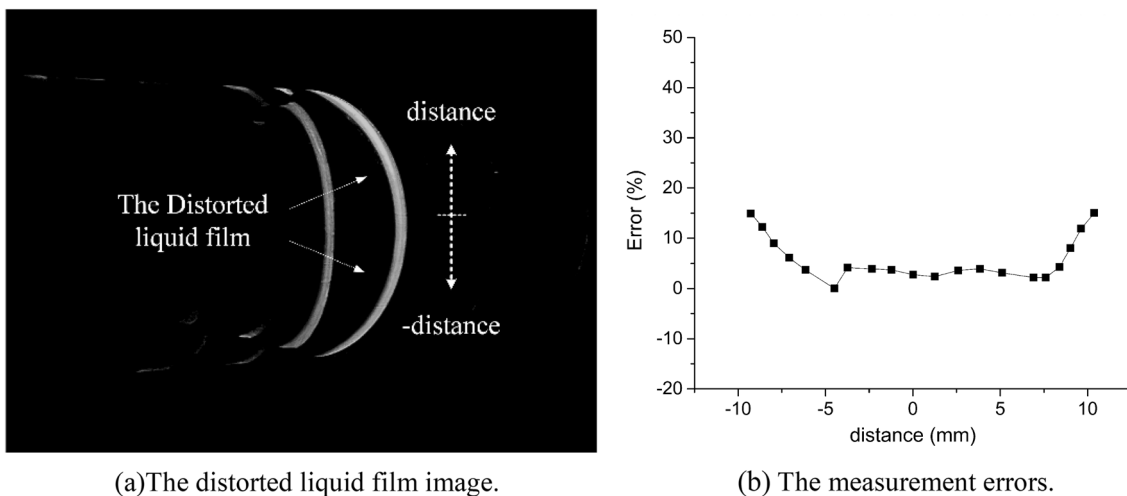


Fig. 5 The static experiment to verify the correction method

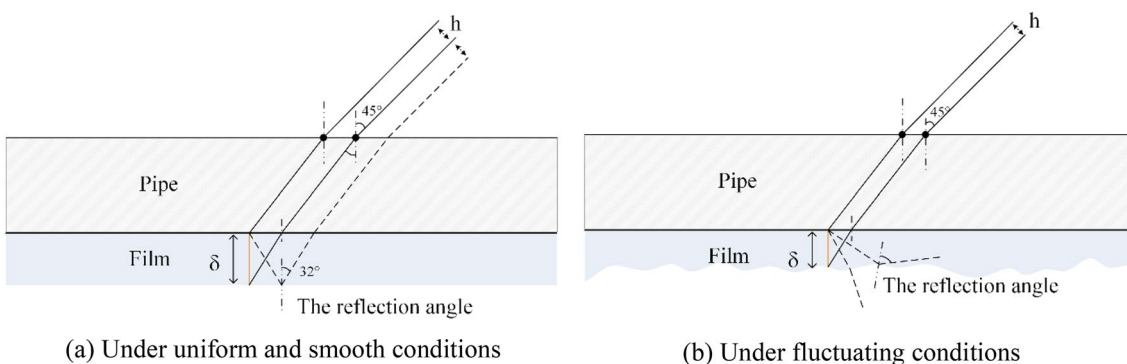


Fig. 6 The effect of total reflection

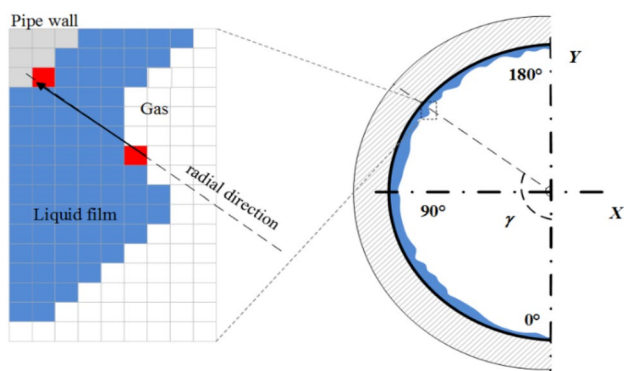


Fig. 7 Circumferential film thickness extraction

angle from the bottom of the pipe. During the extraction process, the circumferential liquid film thickness is represented as the distance between the first and last pixels along the radial direction.

On the basis of these image processing steps, the circumferential film thickness distribution is obtained, and the flow structure can be reconstructed according to the measurement results in the next section.

4 Result and analysis

In order to investigate the mechanism of forming the liquid film at the top of the horizontal pipe, the spatial-temporal flow structure is reconstructed. The liquid film thickness and entrainment concentration characteristics are extracted from the circumferential liquid film images. The Froude number Fr is introduced to describe the liquid film distribution. The gas and liquid superficial velocities, the gas and liquid phase density and the pipe diameter are all considered in Fr number, which represents the ratio of inertial force to gravity. The Fr number modified by Setyawan et al. (2017) is defined as Eq. (1).

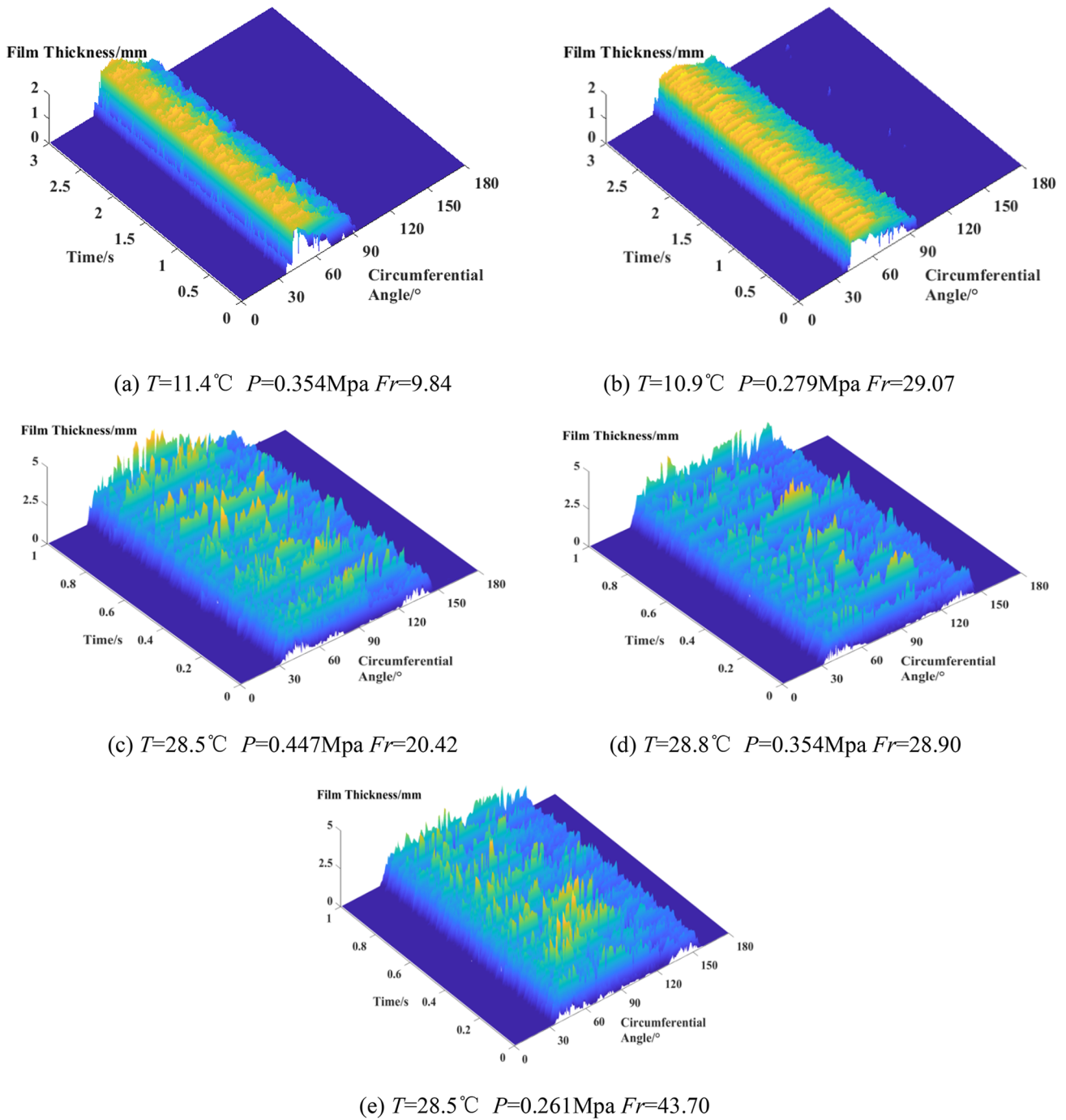


Fig. 8 Spatial–temporal flow structure of circumferential liquid film

$$Fr = \frac{\sqrt{\rho_G}(U_{sg} - U_{sl})}{\sqrt{(\rho_L - \rho_G)(gD)}} \tag{1}$$

where ρ_G and ρ_L denote the densities of gas and liquid, U_{sg} and U_{sl} are the superficial velocities of gas and liquid, g is the acceleration of gravity, and D is the diameter of the pipe.

4.1 Spatial–temporal flow structure reconstruction

Under different gas pressure and temperature conditions, Fig. 8 shows the spatial–temporal distribution of the circumferential film thickness as the Fr increases. The X-axis, Y-axis and Z-axis denote the measured circumferential angle, time and the liquid film thickness, respectively. In Fig. 8a,

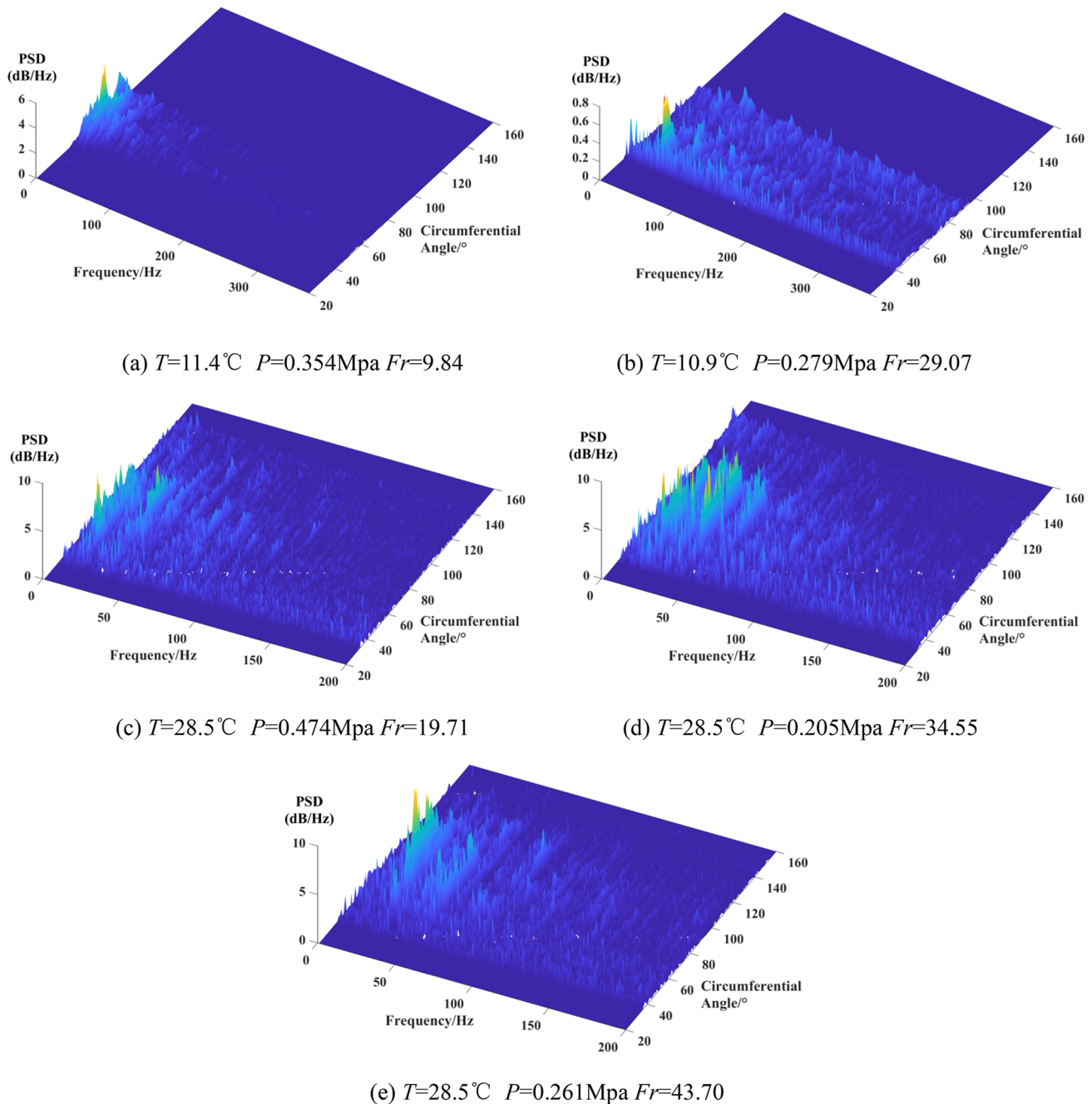


Fig. 9 Circumferential liquid film thickness power density

b, the flow pattern inside the pipe is the wavy flow, where the circumferential film is asymmetrical due to gravity. As the circumferential angle increasing, the liquid film thickness becomes thinner and invisible at about 100° . When the circumferential angle exceeds 100° , droplet deposition can be observed in the upper half of the pipe as shown in Fig. 8b. As the liquid and gas superficial velocities increase, the flow pattern inside the pipe becomes the annular flow, as shown in Fig. 8c–e. It can be observed that the liquid film on the

bottom of the pipe is thicker than that on the top of the pipe. The correspondence analyses in frequency domain for the film thickness are shown as follows.

In Fig. 9, the X-axis, Y-axis and Z-axis denote the circumferential measurement angle, the frequency, the power density of the circumferential liquid film thickness, respectively. Figure 9a, b shows the power density of the wavy flow inside the pipe. When the Fr number is small, the liquid film develops to 90° and the dominant frequency is in the low

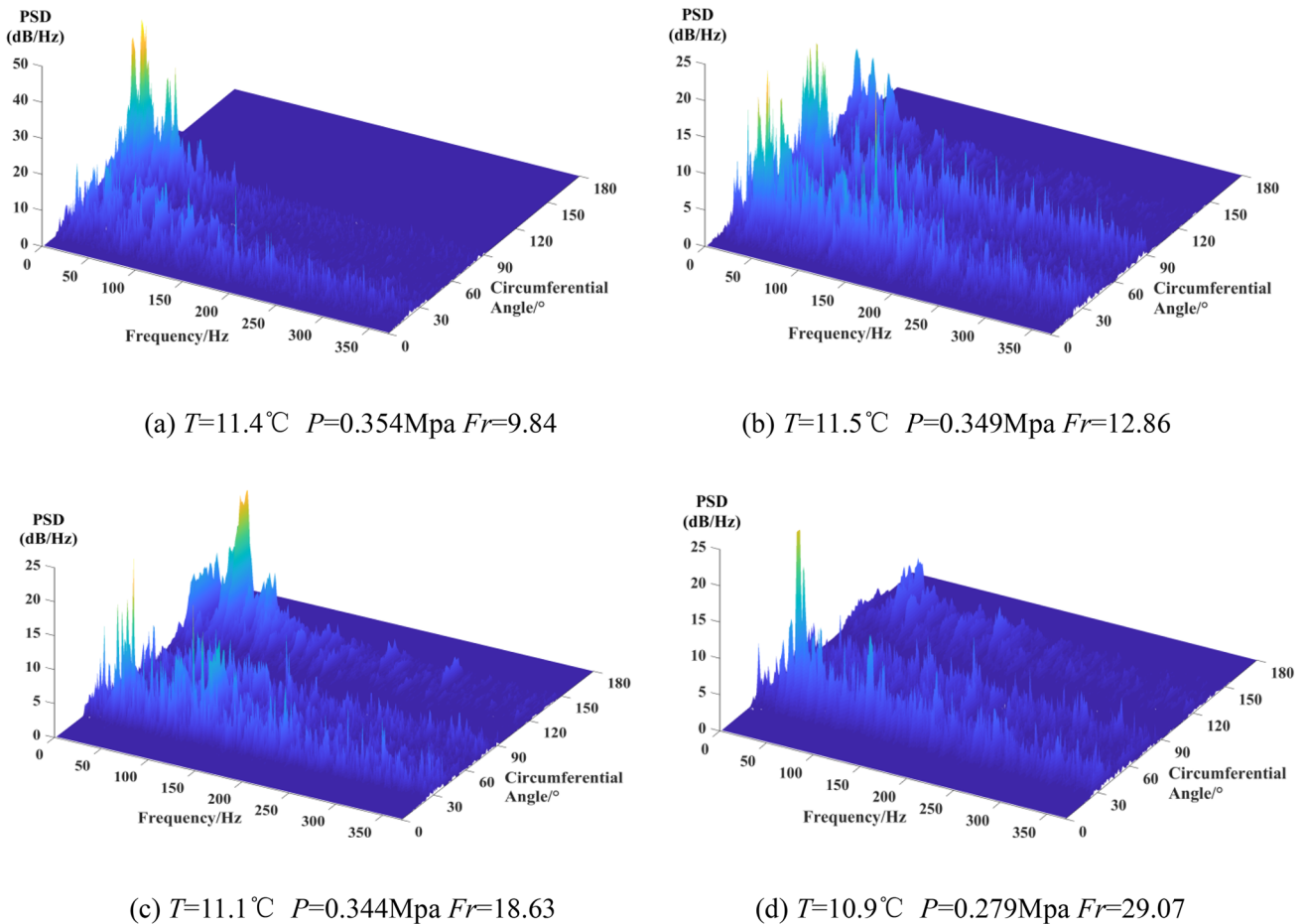


Fig. 10 Circumferential entrainment concentration power density

frequency band. It means that there is no stable liquid film in the upper part of the pipe, and the liquid film is relatively uniform. With the increase in the Fr , the fluctuation of the liquid film increases, but there is still no stable liquid film near the top of the pipe, as shown in Fig. 9b. The power densities of the annular flow are shown in Fig. 9c–e. The dominant frequency of the lower part is in the low frequency band, while the frequency distribution of the upper half is more dispersed, which indicates that the disturbance waves from the lower part do not fully overcome the gravity to supply the liquid film at the top of the pipe. With the increase in the Fr , the dominant frequency of the lower half develops toward higher frequency and the fluctuation of the liquid film enhances.

The mist-like edge caused by the liquid entrainment and deposition can be observed on the surface of the bottom liquid film and the top liquid film, and these areas are extracted as the concentration signal. The power spectra of the concentration signal are shown in Fig. 10, where the Z-axis is the entrainment concentration power density. The

circumferential distribution of the power density is analyzed in the same frequency, and the peaks of the power density appear in the regions of 30° , 80° , and 130° . At the same circumferential angle, the dominant frequency is in the low frequency bands which are smaller than 50 Hz. The frequency distribution of the upper half is similar to that of the lower half, and the low frequency component is retained in the upper part. It means that the entrainment is vital to maintain the liquid film in the upper half of the pipe. With the increase in Fr , the peak value of the power density in the upper half of the pipe increases first and then decreases, which indicates that the droplet deposition near the top of the pipe is changing based on the same rule.

To deeply investigate the circumferential characteristic distribution of annular flow and the formation mechanism of the liquid film near the top of pipe, it is necessary to further analyze the liquid film and entrainment concentration distribution both the upper and lower halves of the horizontal pipe based on the cross-correlation method.

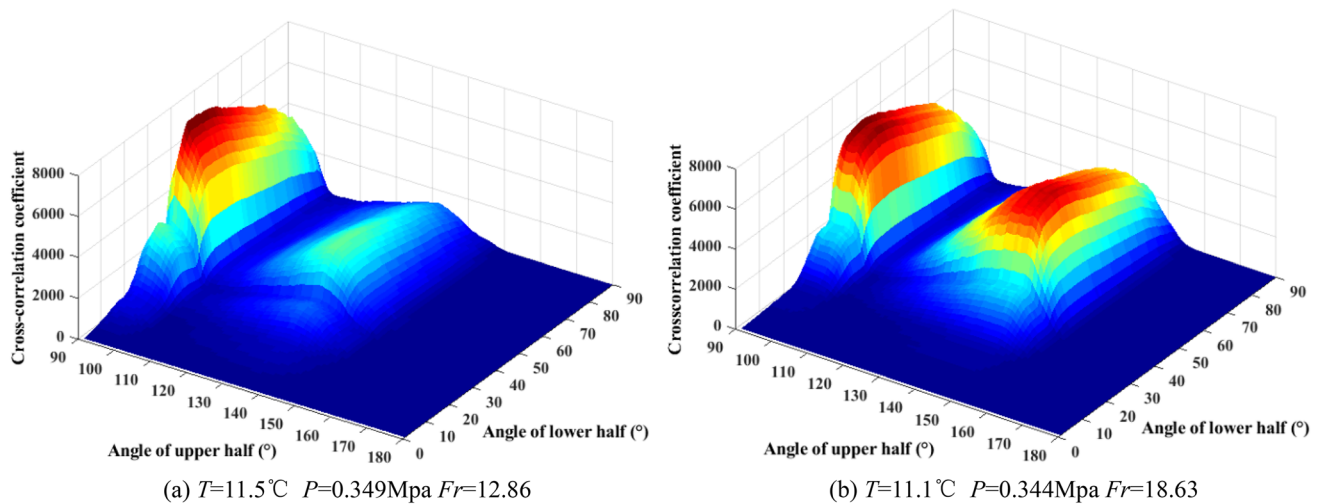


Fig. 11 Cross-correlation coefficient of the entrainment concentration between upper and lower half of the pipe

4.2 Cross-correlation analysis

The cross-correlation coefficient R between the two sets of discrete signals $X(t)$ and $Y(t)$ can be defined as Eq. (2).

$$R = \max_{m \in (-\infty, \infty)} \left(\sum_{t=-\infty}^{\infty} X(t)Y(t-m) \right) \quad (2)$$

Figure 11 shows the relationship of the entrainment concentration between the upper half and lower half of the pipe at each angle in wavy flow, where the Z-axis is the cross-correlation coefficient. The upper half and lower half of the pipe is divided by the circumferential angle of 90° . The results show that the cross-correlation coefficient increases rapidly in the area corresponding to the circumferential angle of $30\text{--}50^{\circ}$ and the $120\text{--}160^{\circ}$. These areas are considered to be related to the droplet formation and the droplet deposition, respectively. With the increase in the Fr , the correlation between the droplet deposition and formation increases rapidly, which indicates the droplet formation in the lower half is the origin of droplet deposition near the top of the pipe.

Figure 12 depicts the cross-correlation of the film thickness between the upper half and lower half of the pipe at each circumferential angle in annular flow. As shown in Fig. 12, the peak corresponds to $30\text{--}50^{\circ}$ in the lower half and $140\text{--}160^{\circ}$ in the upper half, where droplets generate and deposit in wavy flow. The amplitude of cross-correlation peak grows up with the increase in Fr , which indicates that liquid film adhered on the top of the pipe is replenished by the droplet deposition, and the

replenishment is continuously enhanced as the Fr number increasing.

4.3 Liquid film formation analysis

Based on PLIF, the circumferential film can be imaged, and meanwhile, the flow pattern can be confirmed, which helps to comprehend the mechanism of the film formation. To interpret the formation of the liquid film adhered on the top of the pipe, the film images of wavy flow are analyzed under different Fr numbers in Fig. 13. Figure 13a shows that there is no stable liquid film in the upper part of the pipe when Fr is low. With the increase in the Fr , the top of the pipe is gradually wetted. Combined with the spatial–temporal distribution and cross-correlation analysis, the mechanism of forming the liquid film at the top of the horizontal pipe is investigated.

Firstly, compared with the disturbance wave, the liquid entrainment and deposition phenomena are more significant in transition flow pattern. The circumferential liquid film develops to near the 90° , but there is no stable liquid film around 90° as shown in Fig. 13, which means that it is not the disturbance waves that transport the liquid to the top of the pipe. The liquid film and entrainment concentration have been analyzed in the time and frequency domain. According to the frequency domain analyses in Figs. 9 and 10, the contribution of the droplet deposition is more significant than that of wave. Secondly, a corresponding positional relationship can be presented between the droplets entrainment and deposition. Cross-correlation analysis has been performed on the liquid film and entrainment concentration

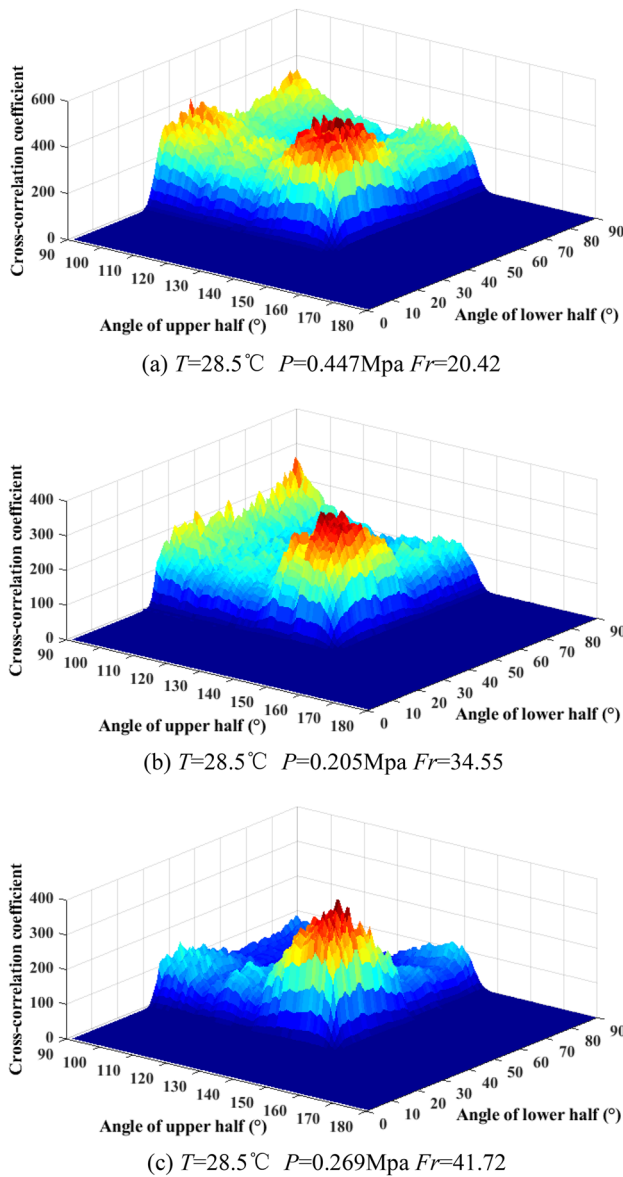


Fig. 12 Cross-correlation coefficient of the liquid film between the upper and lower half of the pipe

between the upper half and lower half of the pipe. Figure 11 shows that the correlation peak corresponds to 30–50° in the lower half and 140–160° in the upper half. Figure 13 also shows that the gas core peels the droplets from the surface of the liquid film in the lower part. Combined with the cross-correlation analysis and the circumferential liquid film images, it is shown that the liquid is stripped from the surface of the liquid film in the lower half of the pipe and transported to the top of the pipe within the gas core. As the droplet deposition increasing, the top of the pipe is gradually wetted and the stable liquid film is formed. Finally, the

entrainment and deposition of droplets also play an important role in maintaining the top liquid film besides the wave spreading in annular flow. Figure 12 shows that the peak of the cross-correlation is the same as the positions where the droplets entrainment and deposition in transition flow pattern as shown in Fig. 11, and the peak increases with Fr , which indicates that liquid film adhered on the top of the pipe is replenished by the droplets. In this paper, the droplet deposition is considered as the main cause of forming the liquid film near the top of pipe in transition flow pattern, and it also contributes to maintaining the liquid film near the top of pipe besides the wave spreading in annular flow, as shown in Fig. 14.

On the basis of mechanism analysis, it is considered that the formation of top liquid film is related to the liquid phase overcoming gravity. The physical parameters affecting the circumferential distribution of the liquid film thickness include U_G , U_L , gravity, gas and liquid density, which play an important role in the process of liquid phase overcoming gravity. The Froude number represents the ratio of inertial force to gravity, so these effects are considered as the Fr . In addition, the thickness of the liquid film is affected by the circumferential angle. Therefore, a model of the liquid film thickness distribution considering Fr and circumferential angle is established. The circumferential distribution is calculated, and the average thickness of the liquid film is varied with the circumferential angle and Fr . In Fig. 15, the red and blue points are the average film thickness, and a fourth-order polynomial model is used to fit it. The blue sets of points are selected to test the model calculated by the red sets. The fitting result is as shown in Eq. (3). The RMSE of the fitting result is 0.176, and the coefficient of determination is 0.7029 (Table 2). The distribution of the circumferential film is accurately represented by the fitting result as shown in Fig. 15b. In Fig. 15a, a peak of film thickness can be found in the upper part of the pipe due to the concentrated deposition of the liquid.

$$f(\theta, Fr) = p_{00} + p_{10}Fr + p_{01}\theta + p_{11}Fr \times \theta + p_{02}\theta^2 + p_{12}Fr \times \theta^2 + p_{03}\theta^3 + p_{13}Fr \times \theta^3 + p_{04} \times \theta^4 \tag{3}$$

5 Conclusion

The circumferential characteristics of the liquid film are dominated to the heat and mass transfer process, and thus, it is significant to measure the circumferential characteristics. In this paper, the circumferential film characteristics are measured accurately based on PLIF. According to the

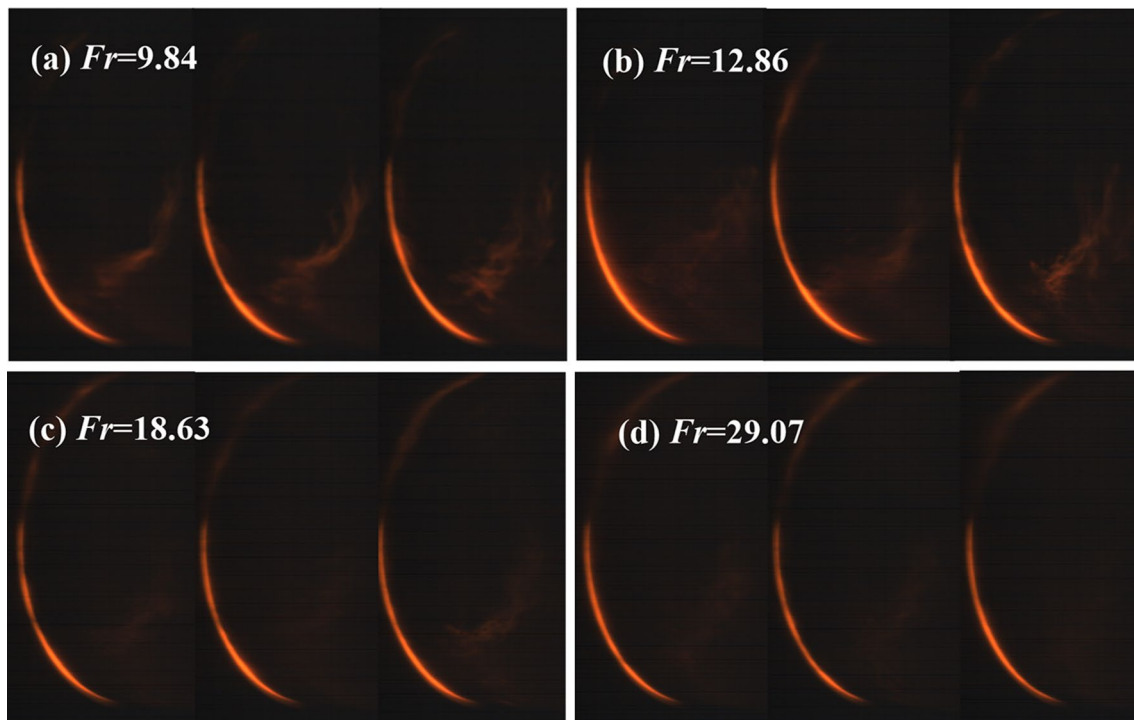


Fig. 13 Circumferential film images with different Fr numbers

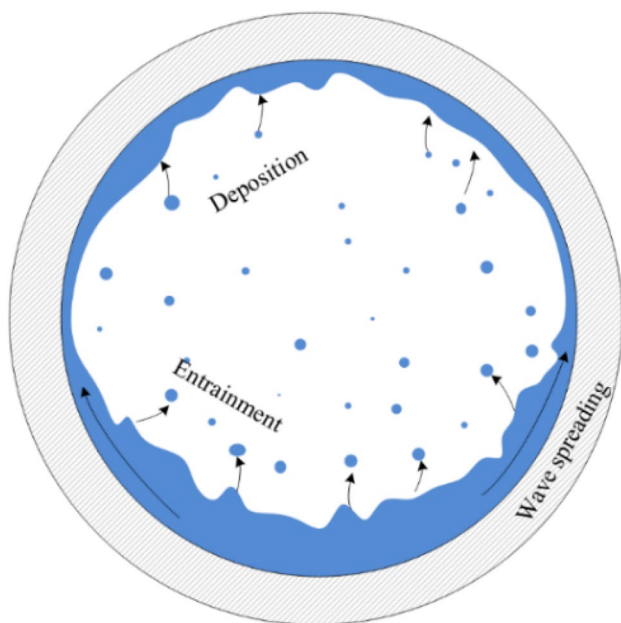
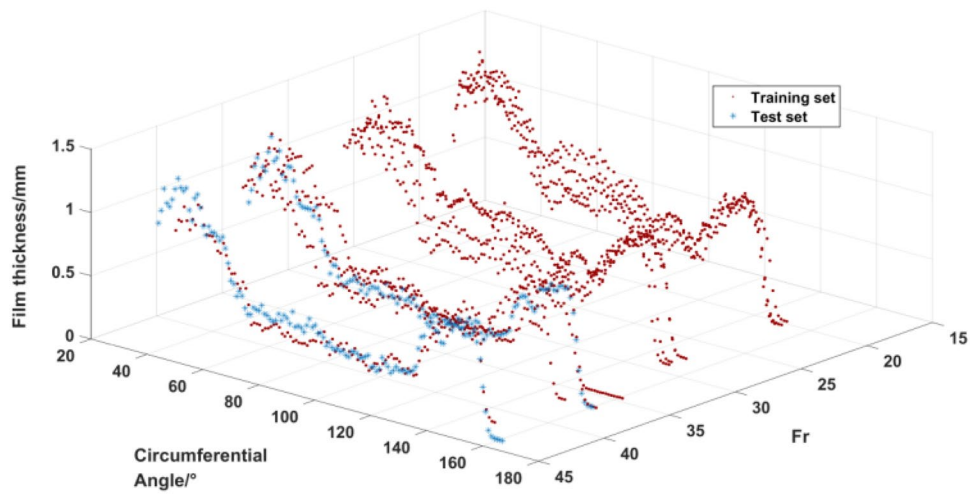


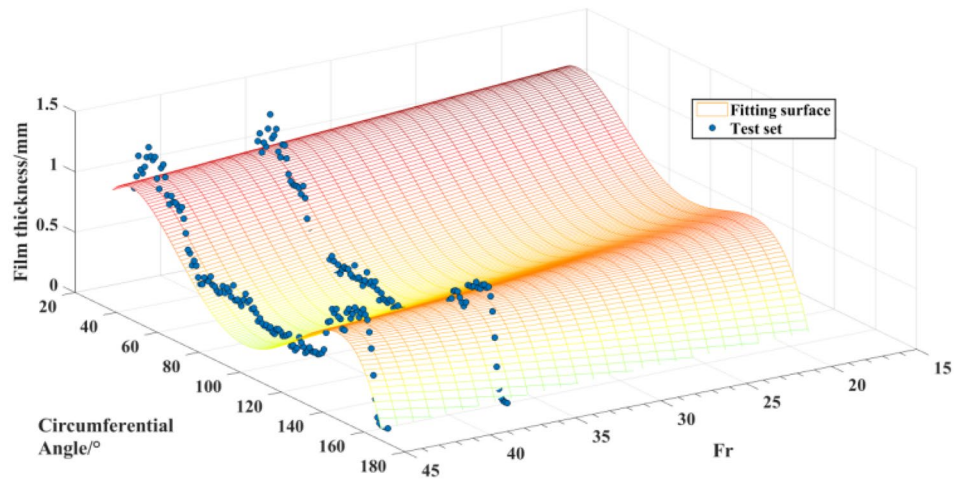
Fig. 14 The formation of the liquid film near the top of pipe

circumferential film thickness, the spatial–temporal flow structure is reconstructed, which is of great significance to analyze the heat and mass transfer efficiency. Moreover, the mechanism of forming the liquid film at the top of the horizontal pipe is also investigated. Based on the cross-correlation analysis, it is discovered that the entrainment concentrations have a corresponding relationship between upper half and lower half in the wavy flow. In transition flow pattern, compared with the disturbance wave, the main cause for the liquid film formation near the top of pipe is the entrainment and deposition phenomena. In annular flow, the entrainment and deposition of droplets also play an important role in maintaining the top liquid film besides the wave spreading. Finally, a model which predicts the circumferential film thickness under different Fr and circumferential angle is established and compared with the measured film thickness to verify the accuracy of the model.

Fig. 15 Liquid film average thickness and circumferential distribution model



(a) Circumferential film average thickness model



(b) Fitting model compared with the test set

Table 2 The coefficients of Eq. (3)

P_{00}	P_{10}	P_{01}	P_{11}	P_{02}	P_{12}	P_{03}	P_{13}	P_{04}
-1.61	-1.14×10^{-2}	0.19	2×10^{-4}	5.30×10^{-8}	-4.08×10^{-3}	-8.85×10^{-6}	3.44×10^{-5}	-1.01×10^{-7}

Acknowledgements This work was supported by the National Natural Science Foundation of China [61671321, 61828106, and 62071325].

References

Alekseenko SV, Antipin VA, Cherdantsev AV et al (2008) Investigation of waves interaction in annular gas-liquid flow using high-speed fluorescent visualization technique. *Micrograv Sci Technol* 20(3):271–275

Alekseenko S, Cherdantsev A, Cherdantsev M et al (2012) Application of a high-speed laser-induced fluorescence technique for studying

the three-dimensional structure of annular gas-liquid flow. *Exp Fluids* 53(1):77–89

Alekseenko SV, Cherdantsev AV, Heinz OM et al (2014) Analysis of spatial and temporal evolution of disturbance waves and ripples in annular gas-liquid flow. *Int J Multiph Flow* 67:122–134

Al-Sarkhi A, Sarica C, Magrini K (2012) Inclination effects on wave characteristics in annular gas-liquid flows. *AIChE J* 58(4):1018–1029

An JS, Cherdantsev AV, Zadrazil I et al (2020) Study of disturbance wave development in downwards annular flows with a moving frame-of-reference brightness-based laser-induced fluorescence method. *Exp Fluids*. <https://doi.org/10.1007/s00348-020-03001-w>

Anderson RJ, Russell TWF (1970) Film formation in two-phase annular flow. *AIChE J* 16(4):626–633

- Berna C, Escrivá A, Muñoz-Cobo JL et al (2014) Review of droplet entrainment in annular flow: interfacial waves and onset of entrainment. *Prog Nucl Energy* 74:14–43
- Charogiannis A, An JS, Voulgaropoulos V, Markides CN (2019) Structured planar laser-induced fluorescence (S-PLIF) for the accurate identification of interfaces in multiphase flows. *Int J Multiph Flow* 118:193–204
- Cherdantsev AV, An JS, Charogiannis A, Markides CN (2019) Simultaneous application of two laser-induced fluorescence approaches for film thickness measurements in annular gas-liquid flows. *Int J Multiph Flow* 119:237–258
- Cioncolini A, Thome JR (2013) Liquid film circumferential asymmetry prediction in horizontal annular two-phase flow. *Int J Multiph Flow* 51:44–54
- Eckeveld AC, Gotfredsen E, Westerweel J, Poelma C (2018) Annular two-phase flow in vertical smooth and corrugated pipes. *Int J Multiph Flow* 109:150–163
- Farias P, Martins F, Sampaio L et al (2012) Liquid film characterization in horizontal, annular, two-phase, gas-liquid flow using time-resolved laser-induced fluorescence. *Exp Fluids* 52(3):633–645
- Fukano T, Ousaka A (1989) Prediction of the circumferential distribution of film thickness in horizontal and near-horizontal gas-liquid annular flows. *Int J Multiph Flow* 15:403–419
- Geraci G, Azzopardi BJ, Maanen HRE (2007) Inclination effects on circumferential film flow distribution in annular gas/liquid flows. *AIChE J* 53(5):1144–1150
- Haber T, Gebretsadik M, Bockhorn H, Zarzalis N (2015) The effect of total reflection in LIF imaging of annular thin films. *Int J Multiph Flow* 76:64–72
- Jayanti S, Hewitt GF, White SP (1990) Time-dependent behaviour of the liquid film in horizontal annular flow. *Int J Multiph Flow* 16(6):1097–1116
- Kattan N, Favrat D, Thome JR (1998) Flow boiling in horizontal tubes: part 2—new heat transfer data for five refrigerants. *J Heat Transfer* 120(1):148–155
- Laurinat JE, Hanratty TJ, Jepson WP (1985) Film thickness distribution for gas-liquid annular flow in a horizontal pipe. *Phys Chem Hydrodyn* 6(1):179–195
- Layssac T, Capo C, Lips S, Mauro AW, Revellin R (2017) Prediction of symmetry during intermittent and annular horizontal two-phase flows. *Int J Multiph Flow* 95:91–100
- Li W, Zhou F, Li R, Zhou L (1999) Experimental study on the characteristics of liquid layer and disturbance waves in horizontal annular flow. *J Therm Sci* 4:235–242
- Lin TF (1985) Film thickness measurements and modeling in horizontal annular flows. *Phys Chem Hydrodyn* 6:197–206
- Mandhane JM, Gregory GA, Aziz K (1974) A flow pattern map for gas-liquid flow in horizontal pipes. *Int J Multiph Flow* 1(4):537–553
- Mauro AW, Cioncolini A, Thome JR, Mastrullo R (2014) Asymmetric annular flow in horizontal circular macro-channels: basic modeling of liquid film distribution and heat transfer around the tube perimeter in convective boiling. *Int J Heat Mass Transf* 77:897–905
- Morgan RG, Markides CN, Hale CP et al (2012) Horizontal liquid-liquid flow characteristics at low superficial velocities using laser-induced fluorescence. *Int J Multiph Flow* 43:101–117
- Morgan RG, Markides CN, Zadzrazil I et al (2013) Characteristics of horizontal liquid-liquid flows in a circular pipe using simultaneous high-speed laser-induced fluorescence and particle velocimetry. *Int J Multiph Flow* 49:99–118
- Schubring D, Shedd TA, Hurlburt ET (2010) Planar laser-induced fluorescence (PLIF) measurements of liquid film thickness in annular flow. Part II: analysis and comparison to models. *Int J Multiph Flow* 36:825–835
- Schubring D, Ashwood AC, Shedd TA, Hurlburt ET (2010) Planar laser-induced fluorescence (PLIF) measurements of liquid film thickness in annular flow. Part I: methods and data. *Int J Multiph Flow* 36:815–824
- Schubring D, Shedd TA (2009) Critical friction factor modeling of horizontal annular base film thickness. *Int J Multiph Flow* 35(4):389–397
- Setyawan A, Indarto D (2017) Experimental investigations of the circumferential liquid film distribution of air-water annular two-phase flow in a horizontal pipe. *Exp Thermal Fluid Sci* 85:95–118
- Westende JMCV, Belt RJ, Portela LM, Mudde RF, Oliemans RVA (2007) Effect of secondary flow on droplet distribution and deposition in horizontal annular pipe flow. *Int J Multiph Flow* 33(1):67–85
- Xue T, Zhang S (2018) Investigation on heat transfer characteristics of falling liquid film by planar laser-induced fluorescence. *Int J Heat Mass Trans* 126:715–724
- Xue T, Zhou C, Lin X (2017) Circumference liquid film measurement method with single high-speed camera. 2017 IEEE international instrumentation and measurement technology conference (I2MTC). pp 1–5
- Xue T, Li C, Wang Q (2019b) Optical analysis and correction for circumferential liquid film measurement based on planar laser-induced fluorescence method. 2019 IEEE international instrumentation and measurement technology conference (I2MTC). pp 1–5
- Xue T, Li C, Wu B (2019) Distortion correction and characteristics measurement of circumferential liquid film based on PLIF. *AIChE J* 65:e16612
- Zadzrazil I, Markides CN (2014) An experimental characterization of liquid films in downwards co-current gas-liquid annular flow by particle image and tracking velocimetry. *Int J Multiph Flow* 67:42–53
- Zadzrazil I, Matar OK, Markides CN (2014) An experimental characterization of downwards gas-liquid annular flow by laser-induced fluorescence: flow regimes and film statistics. *Int J Multiph Flow* 60:87–102

Publisher's Note Springer Nature remains neutral with regard to jurisdictional claims in published maps and institutional affiliations.

Authors and Affiliations

Ting Xue¹ · Tao Zhang¹ · Chenyang Li¹ · Zhuping Li¹

¹ Tianjin Key Laboratory of Process Measurement and Control, College of Electrical and Information Engineering, Tianjin University, Tianjin 300072, China